



**HAL**  
open science

## Development of a novel fluorescent ligand of growth hormone secretagogue receptor based on the N-Terminal Leap2 region

Franco Barrile, Céline M’Kadmi, Pablo de Francesco, Agustina Cabral, Guadalupe García Romero, Emilio Mustafá, Sonia Cantel, Marjorie Damian, Sophie Mary, Séverine Denoyelle, et al.

### ► To cite this version:

Franco Barrile, Céline M’Kadmi, Pablo de Francesco, Agustina Cabral, Guadalupe García Romero, et al.. Development of a novel fluorescent ligand of growth hormone secretagogue receptor based on the N-Terminal Leap2 region. *Molecular and Cellular Endocrinology*, 2019, 498, pp.110573. 10.1016/j.mce.2019.110573 . hal-02375522

**HAL Id: hal-02375522**

**<https://hal.science/hal-02375522>**

Submitted on 20 Jul 2022

**HAL** is a multi-disciplinary open access archive for the deposit and dissemination of scientific research documents, whether they are published or not. The documents may come from teaching and research institutions in France or abroad, or from public or private research centers.

L’archive ouverte pluridisciplinaire **HAL**, est destinée au dépôt et à la diffusion de documents scientifiques de niveau recherche, publiés ou non, émanant des établissements d’enseignement et de recherche français ou étrangers, des laboratoires publics ou privés.



Distributed under a Creative Commons Attribution - NonCommercial 4.0 International License



29 **ABSTRACT**

30

31 Liver-expressed antimicrobial peptide 2 (LEAP2) was recently recognized as an  
32 endogenous ligand for the growth hormone secretagogue receptor (GHSR), which also is a  
33 receptor for the hormone ghrelin. LEAP2 blocks ghrelin-induced activation of GHSR and  
34 inhibits GHSR constitutive activity. Since fluorescence-based imaging and pharmacological  
35 analyses to investigate the biology of GHSR require reliable probes, we developed a novel  
36 fluorescent GHSR ligand based on the N-terminal LEAP2 sequence, hereafter named F-  
37 LEAP2. *In vitro*, F-LEAP2 displayed binding affinity and inverse agonism to GHSR similar to  
38 LEAP2. In a heterologous expression system, F-LEAP2 labeling was specifically observed in  
39 the surface of GHSR-expressing cells, in contrast to fluorescent ghrelin labeling that was  
40 mainly observed inside the GHSR-expressing cells. In mice, centrally-injected F-LEAP2  
41 reduced ghrelin-induced food intake, in a similar fashion to LEAP2, and specifically labeled  
42 cells in GHSR-expressing brain areas. Thus, F-LEAP2 represents a valuable tool to study the  
43 biology of GHSR *in vitro* and *in vivo*.

44

45 **Keywords:** ghrelin, G-protein coupled receptor, inverse agonist, fluorescent probe.

46

## 47 1. INTRODUCTION

48

49 The growth hormone secretagogue receptor (GHSR) is a prototypical class A G protein  
50 coupled receptor (GPCR) (Howard et al., 1996). Ghrelin, a gastrointestinal tract-derived  
51 octanoylated 28-residue peptide hormone, was the first known endogenous ligand for GHSR  
52 (Kojima et al., 1999). Recently, liver-expressed antimicrobial peptide 2 (LEAP2) was  
53 recognized as another endogenous ligand for GHSR (Ge et al., 2018). Ghrelin activates GHSR  
54 signaling, while LEAP2 acts as both antagonist and inverse agonist of GHSR (Ge et al., 2018;  
55 M'Kadmi et al., 2019; Wang et al., 2019). GHSR also exerts ligand-independent actions as it  
56 displays a high constitutive activity, which reaches ~50% of its maximal activity, and can  
57 heterodimerize with other GPCRs in order to affect their activity (Kern et al., 2015, 2012;  
58 Schellekens et al., 2015). GHSR regulates key physiological functions in humans. For  
59 instance, up-regulation of GHSR signaling potently increases growth hormone (GH) secretion  
60 and promotes mechanisms that increase glycaemia (Garin et al., 2013). Ghrelin-induced  
61 activation of GHSR also potently and rapidly stimulates food intake (Garin et al., 2013).  
62 Notably, GHSR is highly expressed in the brain and, consequently, regulates a variety of  
63 central functions including reward-related cognition, associative learning, memory, stress  
64 responses, among others (Morin et al., 2018; Perello and Dickson, 2015). Thus, GHSR is a  
65 highly attractive drug target to treat a variety of pathological conditions in human beings.

66

67 Development of fluorescent GPCR ligands is a major topic in pharmacology for *in vitro*  
68 and *in vivo* applications (Iliopoulos-Tsoutsouvas et al., 2018). The use of fluorescently-labeled  
69 ghrelin was essential to study the localization, function and regulation of GHSR. In particular,  
70 we reported the first fluorescence-based ligand binding assay for GHSR relying on  
71 fluorescence resonance energy transfer (FRET) between fluorescent versions of GHSR and  
72 ghrelin (Degorce et al., 2009; Keppler et al., 2004; Leyris et al., 2011; Maurel et al., 2008). We  
73 also used fluorescent variants of ghrelin to gain insights about different aspects of the  
74 physiology or cell biology of GHSR, including its neuroanatomical distribution in the mouse  
75 brain (Cabral et al., 2013; Cornejo et al., 2018; Fernandez et al., 2016), its regulation by  
76 changes in the energy balance (Fernandez et al., 2018), its subcellular localization in neurons  
77 (Cabral et al., 2016), its cellular trafficking in *in vitro* systems (López Soto et al., 2015) and its  
78 ability to interact with plasma proteins and other GPCRs (Lufrano et al., 2016; Schellekens et  
79 al., 2015). In addition, fluorescently-labeled ghrelin was instrumental to clarify the mechanisms  
80 transporting ghrelin into the brain (Cabral et al., 2017, 2014; Schaeffer et al., 2013; Uriarte et  
81 al., 2019). Still, ghrelin-derived fluorescent probes have some limitations as tools to investigate  
82 the biology of GHSR. First, ghrelin half-life *in vivo* is very short because the ester bond that  
83 links the n-octanoyl moiety to serine<sup>3</sup> is susceptible to be hydrolyzed either spontaneously or

84 by plasma esterases, and des-acyl ghrelin displays a very poor affinity for GHSR (De Vriese  
85 et al., 2007; Hosoda et al., 2000). In order to avoid this limitation, serine<sup>3</sup> of ghrelin sequence  
86 can be replaced by either 3,4-diaminopropionic acid or aspartic acid, which are then linked  
87 through an amide bond with octanoic acid or octylamine, respectively (Leyris et al., 2011;  
88 McGirr et al., 2011). These modifications appear to have a minimal impact on the interaction  
89 of the probes with GHSR (Leyris et al., 2011; McGirr et al., 2011); however, they add an extra  
90 level of complexity in their biosynthesis. Another feature regarding the use of fluorescently-  
91 labeled ghrelin to investigate the biology of GHSR is the ability of ghrelin to promote GHSR  
92 internalization and recycling in living cells (Camiña et al., 2004). These cellular mechanisms  
93 may interfere with the accurate estimation of FRET signal or reduce the sensitivity of  
94 fluorescent assays in some experimental designs. Finally, development of fluorescent probes  
95 with a pharmacological profile different of the natural agonist ligand would be useful for the  
96 analysis of ligand binding or dimerization properties of GHSR. Recently, we established that  
97 LEAP2 binds to the orthosteric site of GHSR and that the N-terminal part of LEAP2 is sufficient  
98 to bind to GHSR and reduce its constitutive activity (M'Kadmi et al., 2019). Importantly, LEAP2  
99 should not promote GHSR internalization due to its pharmacological properties and, as a  
100 consequence, could label GHSR without any effect on its localization. Thus, we decided to  
101 develop a new fluorescent GHSR ligand based on the N-terminal sequence of LEAP2 that  
102 should prove of paramount interest to characterize the molecular behavior of GHSR and to  
103 investigate not only the physiology and cell biology of GHSR but also specific aspects inherent  
104 to the biology of LEAP2.

## 105 2. MATHERIAL AND METHODS

106

107 **2.1. F-LEAP2 synthesis.** H-<sup>1</sup>Nle-<sup>2</sup>Thr-<sup>3</sup>Pro-<sup>4</sup>Phe-<sup>5</sup>Trp-<sup>6</sup>Arg-<sup>7</sup>Gly-<sup>8</sup>Val-<sup>9</sup>Ser-<sup>10</sup>Leu-<sup>11</sup>Arg-  
108 <sup>12</sup>Pro-<sup>13</sup>Ile-<sup>14</sup>Gly-<sup>15</sup>Ala-<sup>16</sup>Ser-<sup>17</sup>Cys-NH<sub>2</sub> was synthesized by solid-phase peptide synthesis  
109 starting from Agilent Amphisphere 40 RAM resin using Fmoc chemistry, HATU/DIEA system  
110 for coupling and piperidine/DMF for deprotection. All coupling steps (5 eq.) were performed  
111 twice for 10 min, with the exception of Fmoc-Thr<sup>2</sup>(tBu)-OH which was coupled twice for 15 min.  
112 Final deprotection was performed with a TFA/TIS/H<sub>2</sub>O (95/2.5/2.5) mixture for 3 h. After  
113 purification by preparative RP-HPLC, the peptide (0.845 eq.) was dissolved in 1 mL of sodium  
114 phosphate solution (pH 7) and conjugated with 1 mg of DY-647P1-maleimide (Dyomics, Jena,  
115 Germany) for 3 h. The fluorescent peptide was directly injected on a preparative RP-HPLC  
116 column and purified. Their identity and purity were evaluated by mass spectrometry analyses.  
117 Preparative RP-HPLC was run on a Gilson PLC 2250 Purification system (Villiers le Bel,  
118 France) instrument using a preparative column (Waters DeltaPak C18 Radial-Pak Cartridge,  
119 100 Å, 40-100 mm, 15 µm particle size) in gradient mode with a flow rate 50.0 mL/min. Buffer  
120 A was 0.1% TFA in water, and buffer B was 0.1% TFA in acetonitrile.

121

122 **2.2. LC/MS analyses.** The LC/MS system consisted of a HPLC-ZQ (Waters) or UPLC  
123 Acquity H-Class (Waters) coupled to a Synapt G2-S (Waters) equipped with an ESI source.  
124 Analyses were carried out using a Phenomenex Kinetex column (C18, 100 Å, 100x2.1 mm,  
125 2.6µm). A flow rate of 0.5 mL/min and a gradient of 0-100% B in 5 min were used: eluent A,  
126 water/0.1% HCO<sub>2</sub>H; eluent B, ACN/0.1% HCO<sub>2</sub>H. Positive-ion electrospray (ESI+) mass  
127 spectra were acquired from 100 to 1500 m/z with a scan time of 0.2 s. Nitrogen was used for  
128 both the nebulizing and drying gas.

129

130 **2.3. MALDI MS and MS/MS Analyses.** Samples were analyzed from CHCA or SA  
131 matrix deposits, in positive ion mode the Rapiflex instrument from Bruker Daltonics®. A pulsed  
132 Nd:YAG laser at a wavelength of 355 nm was operated at a 66.7 Hz frequency with a laser  
133 focus of 29%. Data were acquired with the Flex Control software (version 4.1, Bruker  
134 Daltonics®). Spectra were integrated with the Flex Analysis software (version 4.0,  
135 BrukerDaltonics®), the centroid algorithm was used to assign peaks. An acceleration voltage  
136 of 25.0 kV (IS1) was applied for a final acceleration of 21.95 kV (IS2) and a lense voltage of  
137 9.6 kV. The reflectron mode was used for the ToF analyser (voltages of 26.3 kV and 13.8 kV).  
138 The delayed extraction time was 30 ns. Acquisitions were performed using a reflector detector  
139 voltage of 1.722 kV. MS data were processed with the Flex Analysis software (version 4.0,  
140 Bruker Daltonics®). External calibration was performed with commercial peptide mixture  
141 (Calibration peptide standard II, protein I, Bruker Daltonics, Wissembourg, France).

142 Fragmentation experiments were performed under laser induced dissociation (LID) conditions  
143 with the LIFT cell voltage parameters set at 19.0 kV (LIFT 1) and 3.7 kV (LIFT 2) for a final  
144 acceleration of 29.5 kV (reflector voltage) and a pressure in the LIFT cell around  $4 \times 10^{-7}$  mbar.  
145 The precursor ion selector was set manually to the first monoisotopic peak of the molecular  
146 ion pattern for all analyses. MS/MS data were processed with the Flex Analysis software  
147 (version 4.0, Bruker Daltonics®). Mass lists were generated according to the following  
148 parameters: SNAP as peak detection algorithm, S/N threshold 3.

149

150 **2.4. Drugs.** Ghrelin was purchased from Global Peptides (cat# PI-G-03). Full-length  
151 LEAP2 and LEAP2(1-14)-NH<sub>2</sub> were synthesized, purified by RP-HPLC and characterized by  
152 LC-MS and MALDI-MS/MS with a purity > 95%, as described previously (M'Kadmi et al., 2019).  
153 Fluorescent ghrelin (hereafter named F-ghrelin) was a variant of ghrelin conjugated to DY-  
154 647P1 fluorophore through a C-terminal Cys, as described above for F-LEAP2. Specifically,  
155 F-ghrelin was synthesized by linking DY-647P1-maleimide to a 19-residues ghrelin analog that  
156 contains the initial 18 residues of the ghrelin sequence, but replacing the serine in position 3  
157 by aspartic acid whose side-chain was amidated with amino-octanoic acid, and cysteine at the  
158 position 19. F-ghrelin was purified by RP-HPLC and characterized by LC-MS and MALDI-  
159 MS/MS with a purity > 95%, as described above for F-LEAP2.

160

161 **2.5. Saturation binding assay.** This assay is based on the Tag-lite technology that  
162 combines homogeneous time-resolved fluorescence (HTRF) detection with a covalent labeling  
163 technology called SNAP-tag (Degorce et al., 2009; Keppler et al., 2004; Maurel et al., 2008).  
164 Specifically, F-LEAP2 was used as HTRF acceptor, and GHSR fused with the SNAP-tag  
165 enzyme (SNAP-GHSR) and covalently labeled with a terbium cryptate (Lumi4-Tb) was used  
166 as a HTRF donor (Leyris et al., 2011). HEK293T cells expressing the SNAP-GHSR were  
167 incubated with increasing concentrations of F-LEAP2 diluted in the Tag-lite labelling medium.  
168 For each concentration, nonspecific binding was determined by adding 5  $\mu$ M unlabeled LEAP2  
169 diluted in the same buffer. Plates were incubated for 1 h at room temperature. Two  
170 independent experiments were performed, each of them in triplicate.

171

172 **2.6. *In vitro* assessment of inverse agonist properties of F-LEAP2.** Monomeric  
173 GHSR in lipid nanodiscs and G $\alpha_q$  $\beta_1\gamma_2$  trimer were prepared as previously described (Damian  
174 et al., 2018, 2012). GTP $\gamma$ S binding experiments were carried out using a fluorescent BODIPY-  
175 FL GTP $\gamma$ S analog (McEwen et al., 2001). Association of BODIPY-FL GTP $\gamma$ S to the G protein  
176 was monitored using a fluorescence spectrophotometer (Cary Eclipse, Varian) with the  
177 excitation wavelength set at 500 nm and the emission wavelength at 511 nm. Reaction  
178 conditions were 100 nM G $\alpha_q$ , 500 nM G $\beta_1\gamma_2$ , 100 nM BODIPY-FL GTP $\gamma$ S, and 20 nM GHSR

179 in lipid discs. GHSR, the ligands (ghrelin, LEAP2 or F-LEAP2 at a 10  $\mu$ M final concentration)  
180 and  $G\alpha_q\beta_1\gamma_2$  protein were first incubated for 30 min at room temperature, then BODIPY-FL  
181 GTP $\gamma$ S was added and fluorescence was measured after 10 min incubation at 15°C. Three  
182 independent experiments were performed. Data were presented as the percentage of  
183 maximum BODIPY-FL fluorescence change measured in the presence of ghrelin.

184

185 **2.7. Cell culture imaging studies.** TsA201 cells were plated on glass coverslips  
186 previously treated with poly-L-lysine and laid over 24-well plates. After 24 h, cells growing in  
187 Dulbecco's modified Eagle's medium with 10% fetal bovine serum were transfected with  
188 GHSR-yellow fluorescent protein (YFP)-expressing plasmid using Lipofectamine 2000. After  
189 24 h, cells were pre-incubated with medium alone or containing F-LEAP2 (15 nM) or F-ghrelin  
190 (15 nM) for 15 min. In some cases, cells were pre-incubated with medium alone or containing  
191 LEAP2 (5000 nM) or ghrelin (5000 nM) for 2 min and then exposed to medium containing F-  
192 LEAP2 (15 nM) for 15 min. After that, cells were rinsed with PBS, fixed with 4%  
193 paraformaldehyde in PBS for 30 min, and rinsed again twice with PBS. Finally, glass coverslips  
194 with fixed cells were mounted on glass slides using mounting medium containing Hoechst.  
195 Fluorescent images were acquired using a Zeiss AxioObserver D1 microscope equipped with  
196 an Apotome.2 structured illumination module and an Axiocam 506 monochrome camera. DY-  
197 647P1 was excited at 640 nm and detected in the 690 nm range. YFP was excited at 513 nm  
198 and detected in the 527 nm range. Hoechst was excited at 352 nm and detected in the 460 nm  
199 range. Transfection efficiency was estimated as the ratio between YFP positive cells and the  
200 total number of Hoechst positive cells in fluorescent images acquired at low magnification  
201 (10X/0.45 objective), and represented ~60% in all the experiments. F-LEAP2 and F-ghrelin  
202 signals were estimated in the plasma membrane of YFP positive cells, in fluorescent images  
203 acquired at high magnification (63X/1.4 objective) in 12 cells per condition. The binding of the  
204 fluorescent analogs to the cell surface was estimated as the difference between the total  
205 fluorescent signal at 690 nm of each cell and the internal fluorescent signal at 690 nm in the  
206 same cell (excluding plasma membrane). Specifically, the total area of each cell was first  
207 delimited by manually tracing the boundaries of the cell using the external limits of the GHSR-  
208 YFP fluorescent signal as a reference. Then, the total fluorescence signal intensity at 690 nm  
209 was quantified in the delimited area, as integrated density. Next, the delimited area in each cell  
210 was concentrically reduced by a fixed amount, in order to exclude the green GHSR-YFP  
211 fluorescent signal corresponding to the plasma membrane, and the internal fluorescence  
212 signal intensity at 690 nm was quantified in the reduced area as integrated density. Finally, the  
213 surface fluorescence signal intensity was calculated by subtracting the internal fluorescence  
214 signal from the total fluorescence signal and expressed in arbitrary units (AU). Image analysis  
215 was performed in Fiji (Schindelin et al., 2012).

216

217           **2.8. Mice.** We used adult (8-12 weeks old) male C57BL/6 wild-type mice that were  
218 generated in the animal facility of the IMBICE and housed in a 12-h light/dark cycle with regular  
219 chow and water available *ad libitum*. This study was carried out in strict accordance with the  
220 recommendations in the Guide for the Care and Use of Laboratory Animals of the National  
221 Institutes of Health, and all efforts were made to minimize suffering. All experimentation  
222 received approval from the Institutional Animal Care and Use Committees located in  
223 Multidisciplinary Institute of Cell Biology (approval ID 17-0221).

224

225           **2.9. *In vivo* labeling and neuroanatomical mapping analysis.** Anesthetized mice  
226 were implanted with a single indwelling guide intra-cerebroventricular (ICV) cannula (4 mm  
227 long, 22 gauge, Plastics One) into the lateral ventricle using a stereotaxic. Placement  
228 coordinates were: AP:-0.34 mm; L:+1 mm and V:-2.3 mm. For the *in vivo* experiment 1 (Figure  
229 1A), mice were ICV-injected with 1  $\mu$ L of vehicle (artificial cerebrospinal fluid, n=3) or F-LEAP2  
230 (10 pmol, n=7). For the *in vivo* experiment 2 (Figure 1B), an independent set of mice were first  
231 ICV injected with 1  $\mu$ L of vehicle (n=3), full-length LEAP2 (450 pmol, n=3) or ghrelin (450 pmol,  
232 n=3) and immediately after with 1  $\mu$ L of F-LEAP2 (10 pmol), in order to test the specificity of  
233 the F-LEAP2 labeling. ICV injections were made over 2 min through a 30 gauge needle that  
234 extend 0.5 mm below the guide cannula. The needle was left in place for 2 min, following the  
235 injection, to prevent back flow of the injected solution. After 30 min, anesthetized mice were  
236 perfused with formalin as previously described (Cabral et al., 2012). Brains were extracted,  
237 post-fixed, immersed in 20% sucrose, and coronally cut at 40  $\mu$ m into four equal series on a  
238 cryostat. Correct placement of the cannula was confirmed by histological observation at the  
239 end of the experiment. Brain sections were sequentially mounted on glass slides, coverslipped  
240 with mounting medium containing Hoechst, and imaged in a fluorescence microscope using  
241 structured illumination, as stated above. The presence of F-LEAP2 signal was determined in  
242 1-in-4 series from the level of the olfactory bulbs down to the cervical spinal cord. Fluorescent  
243 images were acquired with a 10X/0.45 objective, using an automated tiling strategy to image  
244 all the brain sections. Also, higher magnification images of selected regions were acquired  
245 using a 40X/0.95 objective. Tiles from each mouse was aligned for neuroanatomical analysis  
246 using the Fiji plugin TrackEM2 (Cardona et al., 2012). The mouse brain atlas of Paxinos and  
247 Franklin (Paxinos and Franklin, 2001) was used to identify brain sections and to describe the  
248 brain nuclei. Estimates of F-LEAP2 signal for the different brain regions were made by  
249 considering both signal strength and number of labeled cells as compared to the signal  
250 observed in negative control samples.

251

252           **2.10. Food intake assessment.** For the *in vivo* experiment 3 (Figure 1C), mice were  
253 permanently implanted with an ICV guide cannula by securing the guide cannulas to the skull  
254 with cranioplastic cement. After surgery, mice were individually housed and allowed to recover  
255 for 5 days. On the morning of the experimental day, *ad libitum* fed mice were ICV-injected, as  
256 described above, with 1  $\mu$ L of vehicle, full-length LEAP2 (10 pmol) or F-LEAP2 (10 pmol) and  
257 immediately after with 1  $\mu$ L of vehicle or ghrelin (60 pmol, n=8 per experimental group). Then,  
258 mice were exposed to a single pre-weighed chow pellet (~1500 mg) in the floor of the home  
259 cages and remained undisturbed. Chow pellets were collected after 2 h and weighed. Weighing  
260 was performed in calibrated scales that had a precision of 1 mg. Two-hour food intake was  
261 calculated subtracting the remaining weight of the pellet to the initial weight, and expressed in  
262 mg.

263  
264           **2.11. Statistical analyses.** Data were expressed as mean $\pm$ SEM. Dissociation constant  
265 of F-LEAP2 was determined from saturation curves of the specific binding. GTP $\gamma$ S binding  
266 experiments and imaging studies were analyzed by ANOVA with Tukey's post-test. Food  
267 intake studies were analyzed by one-way ANOVA test for comparison of different mean values.  
268 Statistical analysis was performed using GraphPad Prism 6.0 software (GraphPad Software,  
269 Inc). Differences were considered statistically significant when  $p < 0.05$ .

### 270 3. RESULTS AND DISCUSSION

271

272 **3.1. Synthesis of F-LEAP2.** The N-terminal LEAP2 sequence was chosen to develop  
273 the fluorescent tracer because it contains the whole bioactive part of the molecule that binds  
274 to GHSR. In order to conjugate LEAP2 to a fluorescent moiety, we decided to take advantage  
275 of the cysteine<sup>17</sup>, which participates in an internal disulfide bridge with cysteine<sup>28</sup> in the native  
276 peptide. Thus, LEAP2(1-17)-NH<sub>2</sub> was first synthesized by solid phase and purified. Then, the  
277 fluorescent probe DY-647P1 was conjugated with the thiol function of cysteine<sup>17</sup> using DY-  
278 647P1-maleimide. The resulting LEAP2(1-17)-DY-647P1 or F-LEAP2 (Figure 2A) was then  
279 purified to homogeneity and confirmed to display the correct molecular mass (theoretical value  
280 2669.2 Da; calculated value 2667.3 Da from observed  $m/z$  1335.1 [M+2H]<sup>2+</sup>,  $m/z$  890.3  
281 [M+3H]<sup>3+</sup>,  $m/z$  668.4 [M+4H]<sup>4+</sup>). Fragmentation experiments confirmed that F-LEAP2 displayed  
282 the correct residue sequence (not shown).

283

284 **3.2. Saturation receptor binding assays for F-LEAP2.** F-LEAP2 binding affinity to  
285 GHSR was estimated using a saturation receptor binding assay. As shown in Figure 2B, F-  
286 LEAP2 bound the living HEK293T cells transiently overexpressing SNAP-GHSR in a typical,  
287 saturable manner, with a calculated dissociation constant of 3.9±1.1 nM. Previously, we found  
288 that full-length LEAP2 and LEAP2(1-14)-NH<sub>2</sub> displayed dissociation constants of 1.3±0.1 and  
289 3.7±0.6 nM, respectively (M'Kadmi et al., 2019). Thus, F-LEAP2 retained high binding affinity  
290 to GHSR despite the attached fluorescent moiety.

291

292 **3.3. *In vitro* assessment of inverse agonist properties of F-LEAP2.** The ability of F-  
293 LEAP2 to affect GHSR-catalyzed Gq activation was tested using GTPγS binding assays. As  
294 shown in Figure 2C, GHSR catalyzed GDP-to-GTP exchange on the Gγ subunit of the Gα<sub>q</sub>β<sub>1</sub>γ<sub>2</sub>  
295 trimer in the absence of ligand, in agreement with its demonstrated high constitutive activity  
296 (Damian et al., 2012). As expected, ghrelin further enhanced GPTγS binding. Unlabeled  
297 LEAP2(1-14)-NH<sub>2</sub> decreased basal GPTγS binding, consistent with the inverse agonist  
298 properties of LEAP2 N-terminal region (M'Kadmi et al., 2019). Similarly, F-LEAP2 decreased  
299 GPTγS binding, indicating that the fluorophore did not affect the inverse agonist properties of  
300 the tracer.

301

302 **3.4. Cell culture imaging studies.** In order to test the ability of F-LEAP2 to label  
303 GHSR-expressing cells, GHSR-YFP-expressing cells were incubated with F-LEAP2 and  
304 visualized in a fluorescence microscope. As shown in Figure 3, F-LEAP2 exclusively bound to  
305 GHSR-YFP-expressing cells and did not bind to nontransfected cells, which lack GHSR-YFP  
306 expression. Notably, F-LEAP2 signal was limited to the cell surface. As shown in Figure 3, F-

307 ghrelin also exclusively labeled GHSR-YFP-expressing cells. In contrast to F-LEAP2, F-ghrelin  
308 signal was mainly localized inside the GHSR-YFP-expressing cells and with a punctuated  
309 pattern that co-localizes with YFP signal. These observations indicate that F-ghrelin induces  
310 internalization of GHSR, as previously reported (Holliday et al., 2007), while F-LEAP2 does  
311 not mediate internalization of the receptor. As also shown in Figure 3, pre-incubation of GHSR-  
312 YFP-expressing cells with an excess of LEAP2 or ghrelin fully prevented the F-LEAP2 binding,  
313 further confirming that F-LEAP2 specifically binds to GHSR. Fluorescence intensity in the  
314 plasma membrane for these conditions was as follows: without fluorescent ligands= $0\pm353$  AU,  
315 F-LEAP2= $15134\pm3764$  AU, F-ghrelin= $1531\pm311$  AU, ghrelin plus F-LEAP2= $2071\pm670$  AU and  
316 LEAP2 plus F-LEAP2= $229\pm370$  AU ( $p<0.0001$  for all the conditions compared to F-LEAP2).  
317 Thus, F-LEAP2 retained high specificity to GHSR despite the attached fluorescent moiety.  
318 Interestingly, it has been shown that the substance P analogue, which was the first reported  
319 GHSR inverse agonist (Holst et al., 2003), also fails to induce internalization of GHSR (Holliday  
320 et al., 2007). Thus, LEAP2 not only blocks ghrelin-evoked activity and reduces constitutive  
321 GHSR activity but also reduces internalization.

322

323 **3.5. *In vivo* imaging studies.** In order to test the capability of F-LEAP2 to label GHSR-  
324 expressing neurons *in vivo*, mice were ICV-injected with F-LEAP2 or vehicle (*In vivo*  
325 experiment 1). After 15 min, mice were euthanized and perfused, and brains were extracted,  
326 frozen, coronally cut and visualized in a fluorescence microscope. The brain areas displaying  
327 significant F-LEAP2 labeling are outlined in Table 1 and summarized with some representative  
328 images in Figure 4. The abbreviations used in the figures and throughout the text are listed in  
329 Table 2. In contrast to vehicle-injected mice, F-LEAP2-injected mice showed labeled cells in a  
330 variety of brain regions. The highest number and strongest intensity of F-LEAP2 labeled cells  
331 were observed in the hypothalamus, with the ARC as the area with highest amount of F-LEAP2  
332 labeled cells (Fig. 4Aa). A relatively high number of F-LEAP2 labeled cells was found in some  
333 specific hypothalamic nuclei, such as the VMH (Fig. 4Ab), VMPO (Fig. 4B), SCh (Fig. 4C),  
334 PVH (Fig. 4D) and SuM (Fig. 4E), while a rather moderate number of F-LEAP2 labeled cells  
335 was found in hypothalamic nuclei, such as the AHA, DMH, Pe and PMV. F-LEAP2 labeled  
336 cells were also found in the DG and the Ammon's horns of the hippocampus (Fig. 4F), in the  
337 MS of the septum (Fig. 4G), in PV of the thalamus and in the SFO (Fig. 4H). A relatively high  
338 number of F-LEAP2-labeled cells was also found in the LDTg (Fig. 4I), which is located at the  
339 junction of the midbrain and pons. In the medulla oblongata, F-LEAP2 labeled cells were  
340 observed in all three components of the dorsal vagal complex: the AP, the NTS and the DMV  
341 (Fig. 4J). The pattern of labeling observed in F-LEAP2-injected mice in all the above referred  
342 brain regions is consistent with previous reports describing the distribution of GHSR mRNA in  
343 mice (Mani et al., 2014; Perello et al., 2012; Zigman et al., 2006) as well as with the pattern of

344 labeling observed in mice ICV injected with fluorescent ghrelin (Cabral et al., 2013).  
345 Interestingly, little number or inconsistent presence of F-LEAP2 labeled cells were found in  
346 some brainstem areas, such as the VTA, SN, DR, DTg, EW, Amb and MCPC, where GHSR  
347 mRNA expression has been previously reported (Perello et al., 2012; Scott et al., 2012; Zigman  
348 et al., 2006). Similarly, low labeling has been also observed in these brain areas in mice ICV-  
349 injected with fluorescent ghrelin (Cabral et al., 2013). Recently, we showed that ICV-injected  
350 fluorescent-ghrelin only accesses to few hundred of microns into the brain parenchyma (Uriarte  
351 et al., 2019). Thus, it seems likely that molecules present in the cerebrospinal fluid cannot  
352 easily reach brain areas distantly located from the brain ventricular system(Perello et al., 2018).  
353 Finally, it is worth mentioning that F-LEAP2 labeling was detected in the cell body and the  
354 cellular processes of hypothalamic tanycytes, which line the floor of the third ventricle (Fig  
355 4Ac), and in epithelial cells of the choroid plexus (Fig 4Fc). This observation is interesting  
356 because these cells form the blood-cerebrospinal fluid barrier and have been proposed to  
357 transport hormones, including ghrelin (Cabral et al., 2015), through these compartments.

358

359 In order to assess the specificity of F-LEAP2 labeling *in vivo*, mice were first ICV-  
360 injected with vehicle, full-length LEAP2 or ghrelin and afterwards with F-LEAP2 (*In vivo*  
361 experiment 2). After 15 min, mouse brains were obtained, as described above, and the F-  
362 LEAP2 signal was estimated in the ARC. In this case, the ARC of mice pretreated with full-  
363 length LEAP2 or ghrelin showed significantly lower F-LEAP2 labeling, as compared to the ARC  
364 of mice pretreated with vehicle (Figure 5). Overall, these data indicated that F-LEAP2 retained  
365 specificity to GHSR in mice.

366

367 **3.6. Bioactivity assessment.** Since LEAP2 inhibits ghrelin-induced food intake, the  
368 bioactivity of F-LEAP2 was estimated by assessing its ability to impair the orexigenic effects  
369 of ghrelin in mice (*In vivo* experiment 3). ICV-injected LEAP2 or F-LEAP2 did not affect food  
370 intake (not shown), while ICV-injected ghrelin potently increases food intake, as it is well  
371 established. In mice pretreated with the LEAP2 variants, ICV-injected F-LEAP2 induced ~40%  
372 reduction of ghrelin-induced food intake, in a similar fashion to that seen for full-length LEAP2  
373 (Figure 6).

374

## 375 4. CONCLUSIONS

376

377 We designed a fluorescent derivative of LEAP2 based on the N-terminal sequence of  
378 the natural peptide, which was confirmed to be the active part of the hormone. The synthesis  
379 F-LEAP2 is easier than the synthesis of fluorescent variants of ghrelin as it does not contain  
380 any posttranslational modification. Since F-LEAP2 does not contain any hydrophobic group,

381 its solubility and handling are also more convenient than probes based on ghrelin. Moreover,  
382 F-LEAP2 is devoid of most non-specific binding effects often associated with ghrelin. F-LEAP2  
383 is fully bioactive and displays high affinity and specificity to GHSR. F-LEAP2 does not induce  
384 GHSR internalization. Since F-LEAP2 is inverse agonist of GHSR signaling while fluorescent  
385 variants of ghrelin are full agonists, F-LEAP2 displays pharmacological properties different to  
386 fluorescent ghrelin. As such, F-LEAP2 extends our palette of pharmacological ligands and  
387 represents a tool of major interest in fluorescent-based pharmacological analyses of GHSR,  
388 including ligand binding and screening assays, dimerization analyzes or tracking of the  
389 diffusion and/or compartmentalization behavior of GHSR at the cell surface. In addition, F-  
390 LEAP2 represents a valuable tool to gain insights about the biology of GHSR in *in vivo* settings.

391 **5. ACKNOWLEDGEMENTS.**

392

393           We would like to thank the support of both the MinCyT-ECOS-Sud program (A13B01)  
394 and the National Agency of Scientific and Technological Promotion of Argentina (PICT2016-  
395 1084 and PICT2017-3196 to MP).

396

397 **6. FIGURE LEGENDS**

398

399 Figure 1: Experimental design of *in vivo* studies. The figure summarizes the experimental  
400 design used for the different studies in which mice received ICV treatments. Panel A depicts  
401 the design of the *in vivo* experiment 1, in which the capability of F-LEAP2 to label the mouse  
402 brain was tested. Panel B depicts the design of the *in vivo* experiment 2, in which the ability of  
403 LEAP2 and ghrelin to block F-LEAP2 labeling in the mouse brain was tested. Panel C depicts  
404 the design of the *in vivo* experiment 3, in which the ability of F-LEAP2 and LEAP2 to impair the  
405 orexigenic effects of ghrelin in mice was assessed.

406

407 Figure 2. Structure and pharmacological features of F-LEAP2. Panel A depicts the structure of  
408 F-LEAP2. Panel B shows saturation binding experiments for F-LEAP2 on HEK293T cells  
409 transiently transfected with SNAP-GHSR. Panel C shows the BODIPY-FL GTP $\gamma$ S binding to  
410 the subunit of G $\alpha_q$  $\beta_1\gamma_2$  induced by GHSR in the absence of ligand or in the presence of ghrelin,  
411 LEAP2(1-14)-NH<sub>2</sub> or F-LEAP2. Data represent the mean $\pm$ SEM. \*\*\*, p $\leq$ 0.001 vs. no ligand  
412 condition.

413

414 Figure 3. F-LEAP2 specifically labels GHSR-expressing cells. First and second columns show  
415 representative microphotographs of GHSR-YFP-expressing tsA201 cells incubated with  
416 medium alone or containing F-LEAP2, respectively. Third column shows representative  
417 microphotographs of GHSR-YFP-expressing tsA201 cells incubated with medium containing  
418 F-ghrelin. Fourth and fifth columns show representative images of GHSR-YFP-expressing  
419 tsA201 cells pre-incubated with LEAP2 or ghrelin, respectively, and then incubated with F-  
420 LEAP2. Arrows point at areas that show co-localization of the fluorescent signals. Asterisks  
421 label cell nuclei of nontransfected cells that lack GHSR-YFP-expression. Scale bar, 10  $\mu$ m.

422

423 Figure 4. F-LEAP2 labels cells in brain areas known to express GHSR. Representative  
424 microphotographs of coronal sections of different brain areas of mice ICV-injected with F-  
425 LEAP2. Insets show high magnification images of the area marked in the low magnification  
426 image. Arrowheads mark different cells labeled with F-LEAP2. Small arrows point at labeled  
427 tanycyte processes. Scale bars: A, 100  $\mu$ m; A a-c, 20  $\mu$ m; B-E, 100  $\mu$ m; F, 200  $\mu$ m; F a-c, 20  
428  $\mu$ m; G-J, 100  $\mu$ m. All abbreviations used for brain nuclei are listed in Table 1.

429

430 Figure 5. F-LEAP2 labeling in the mouse brain is impaired by pretreatment with LEAP2 or  
431 ghrelin. First and second columns show representative photomicrographs of F-LEAP2 signal  
432 in the ARC of mice that were ICV-injected with vehicle alone or containing F-LEAP2,  
433 respectively. Third and fourth columns show representative images of F-LEAP2 signal in the

434 ARC of mice that were ICV-injected with LEAP2 or ghrelin, respectively, and further ICV  
435 injected with F-LEAP2. Insets show high magnification images of the area marked in the low  
436 magnification image. Arrows point F-LEAP2 labeled cells. Scale bars, 100  $\mu$ m (low  
437 magnification), 10  $\mu$ m (high magnification).

438

439 Figure 6. F-LEAP2 blocks ghrelin-induced food intake in a similar fashion as seen for full-length  
440 LEAP2. Food intake in mice ICV injected with vehicle alone or containing LEAP2 or F-LEAP2  
441 and then with ghrelin. Data represent the mean $\pm$ SEM. \*\*,  $p\leq 0.01$ .

442 **7. REFERENCES.**

443

444 Cabral, A., Cornejo, M.P., Fernandez, G., De Francesco, P.N., Garcia-Romero, G., Uriarte,  
445 M., Zigman, J.M., Portiansky, E., Reynaldo, M., Perello, M., 2017. Circulating Ghrelin  
446 Acts on GABA Neurons of the Area Postrema and Mediates Gastric Emptying in Male  
447 Mice. *Endocrinology* 158, 1436–1449. <https://doi.org/10.1210/en.2016-1815>

448 Cabral, A., De Francesco, P.N., Perello, M., 2015. Brain circuits mediating the orexigenic  
449 action of peripheral ghrelin: narrow gates for a vast kingdom. *Front Endocrinol*  
450 (Lausanne) 6, 44. <https://doi.org/10.3389/fendo.2015.00044>

451 Cabral, A., Fernandez, G., Perello, M., 2013. Analysis of brain nuclei accessible to ghrelin  
452 present in the cerebrospinal fluid. *Neuroscience* 253, 406–415.  
453 <https://doi.org/10.1016/j.neuroscience.2013.09.008>

454 Cabral, A., Portiansky, E., Sánchez-Jaramillo, E., Zigman, J.M., Perello, M., 2016. Ghrelin  
455 activates hypophysiotropic corticotropin-releasing factor neurons independently of the  
456 arcuate nucleus. *Psychoneuroendocrinology* 67, 27–39.  
457 <https://doi.org/10.1016/j.psyneuen.2016.01.027>

458 Cabral, A., Suescun, O., Zigman, J.M., Perello, M., 2012. Ghrelin indirectly activates  
459 hypophysiotropic CRF neurons in rodents. *PLoS ONE* 7, e31462.  
460 <https://doi.org/10.1371/journal.pone.0031462>

461 Cabral, A., Valdivia, S., Fernandez, G., Reynaldo, M., Perello, M., 2014. Divergent neuronal  
462 circuitries underlying acute orexigenic effects of peripheral or central ghrelin: critical  
463 role of brain accessibility. *J. Neuroendocrinol.* 26, 542–554.  
464 <https://doi.org/10.1111/jne.12168>

465 Camiña, J.P., Carreira, M.C., El Messari, S., Llorens-Cortes, C., Smith, R.G., Casanueva,  
466 F.F., 2004. Desensitization and endocytosis mechanisms of ghrelin-activated growth  
467 hormone secretagogue receptor 1a. *Endocrinology* 145, 930–940.  
468 <https://doi.org/10.1210/en.2003-0974>

469 Cardona, A., Saalfeld, S., Schindelin, J., Arganda-Carreras, I., Preibisch, S., Longair, M.,  
470 Tomancak, P., Hartenstein, V., Douglas, R.J., 2012. TrakEM2 software for neural  
471 circuit reconstruction. *PLoS ONE* 7, e38011.  
472 <https://doi.org/10.1371/journal.pone.0038011>

473 Cornejo, M.P., De Francesco, P.N., García Romero, G., Portiansky, E.L., Zigman, J.M.,  
474 Reynaldo, M., Perello, M., 2018. Ghrelin receptor signaling targets segregated  
475 clusters of neurons within the nucleus of the solitary tract. *Brain Struct Funct* 223,  
476 3133–3147. <https://doi.org/10.1007/s00429-018-1682-5>

477 Damian, M., Marie, J., Leyris, J.-P., Fehrentz, J.-A., Verdié, P., Martinez, J., Banères, J.-L.,  
478 Mary, S., 2012. High constitutive activity is an intrinsic feature of ghrelin receptor  
479 protein: a study with a functional monomeric GHS-R1a receptor reconstituted in lipid  
480 discs. *J. Biol. Chem.* 287, 3630–3641. <https://doi.org/10.1074/jbc.M111.288324>

481 Damian, M., Pons, V., Renault, P., M’Kadmi, C., Delort, B., Hartmann, L., Kaya, A.I., Louet,  
482 M., Gagne, D., Ben Haj Salah, K., Denoyelle, S., Ferry, G., Boutin, J.A., Wagner, R.,  
483 Fehrentz, J.-A., Martinez, J., Marie, J., Floquet, N., Galès, C., Mary, S., Hamm, H.E.,  
484 Banères, J.-L., 2018. GHSR-D2R heteromerization modulates dopamine signaling  
485 through an effect on G protein conformation. *Proc. Natl. Acad. Sci. U.S.A.* 115, 4501–  
486 4506. <https://doi.org/10.1073/pnas.1712725115>

487 De Vriese, C., Hacquebard, M., Gregoire, F., Carpentier, Y., Delporte, C., 2007. Ghrelin  
488 interacts with human plasma lipoproteins. *Endocrinology* 148, 2355–2362.  
489 <https://doi.org/10.1210/en.2006-1281>

490 Degorce, F., Card, A., Soh, S., Trinquet, E., Knapik, G.P., Xie, B., 2009. HTRF: A technology  
491 tailored for drug discovery - a review of theoretical aspects and recent applications.  
492 *Curr Chem Genomics* 3, 22–32. <https://doi.org/10.2174/1875397300903010022>

493 Fernandez, G., Cabral, A., Andreoli, M.F., Labarthe, A., M’Kadmi, C., Ramos, J.G., Marie, J.,  
494 Fehrentz, J.-A., Epelbaum, J., Tolle, V., Perello, M., 2018. Evidence Supporting a

495 Role for Constitutive Ghrelin Receptor Signaling in Fasting-Induced Hyperphagia in  
496 Male Mice. *Endocrinology* 159, 1021–1034. <https://doi.org/10.1210/en.2017-03101>

497 Fernandez, G., Cabral, A., Cornejo, M.P., De Francesco, P.N., Garcia-Romero, G.,  
498 Reynaldo, M., Perello, M., 2016. Des-Acyl Ghrelin Directly Targets the Arcuate  
499 Nucleus in a Ghrelin-Receptor Independent Manner and Impairs the Orexigenic  
500 Effect of Ghrelin. *J. Neuroendocrinol.* 28, 12349. <https://doi.org/10.1111/jne.12349>

501 Garin, M.C., Burns, C.M., Kaul, S., Cappola, A.R., 2013. Clinical review: The human  
502 experience with ghrelin administration. *J. Clin. Endocrinol. Metab.* 98, 1826–1837.  
503 <https://doi.org/10.1210/jc.2012-4247>

504 Ge, X., Yang, H., Bednarek, M.A., Galon-Tilleman, H., Chen, P., Chen, M., Lichtman, J.S.,  
505 Wang, Y., Dalmás, O., Yin, Y., Tian, H., Jermutus, L., Grimsby, J., Rondinone, C.M.,  
506 Konkar, A., Kaplan, D.D., 2018. LEAP2 Is an Endogenous Antagonist of the Ghrelin  
507 Receptor. *Cell Metab.* 27, 461-469.e6. <https://doi.org/10.1016/j.cmet.2017.10.016>

508 Holliday, N.D., Holst, B., Rodionova, E.A., Schwartz, T.W., Cox, H.M., 2007. Importance of  
509 constitutive activity and arrestin-independent mechanisms for intracellular trafficking  
510 of the ghrelin receptor. *Mol. Endocrinol.* 21, 3100–3112.  
511 <https://doi.org/10.1210/me.2007-0254>

512 Holst, B., Cygankiewicz, A., Jensen, T.H., Ankersen, M., Schwartz, T.W., 2003. High  
513 constitutive signaling of the ghrelin receptor--identification of a potent inverse agonist.  
514 *Mol. Endocrinol.* 17, 2201–2210. <https://doi.org/10.1210/me.2003-0069>

515 Hosoda, H., Kojima, M., Matsuo, H., Kangawa, K., 2000. Ghrelin and des-acyl ghrelin: two  
516 major forms of rat ghrelin peptide in gastrointestinal tissue. *Biochem. Biophys. Res.*  
517 *Commun.* 279, 909–913. <https://doi.org/10.1006/bbrc.2000.4039>

518 Howard, A.D., Feighner, S.D., Cully, D.F., Arena, J.P., Liberatore, P.A., Rosenblum, C.I.,  
519 Hamelin, M., Hreniuk, D.L., Palyha, O.C., Anderson, J., Paress, P.S., Diaz, C., Chou,  
520 M., Liu, K.K., McKee, K.K., Pong, S.S., Chaung, L.Y., Elbrecht, A., Dashkevich, M.,  
521 Heavens, R., Rigby, M., Sirinathsinghji, D.J., Dean, D.C., Melillo, D.G., Patchett, A.A.,  
522 Nargund, R., Griffin, P.R., DeMartino, J.A., Gupta, S.K., Schaeffer, J.M., Smith, R.G.,  
523 Van der Ploeg, L.H., 1996. A receptor in pituitary and hypothalamus that functions in  
524 growth hormone release. *Science* 273, 974–977.  
525 <https://doi.org/10.1126/science.273.5277.974>

526 Iliopoulos-Tsoutsouvas, C., Kulkarni, R.N., Makriyannis, A., Nikas, S.P., 2018. Fluorescent  
527 probes for G-protein-coupled receptor drug discovery. *Expert Opin Drug Discov* 13,  
528 933–947. <https://doi.org/10.1080/17460441.2018.1518975>

529 Keppler, A., Kindermann, M., Gendreizig, S., Pick, H., Vogel, H., Johnsson, K., 2004.  
530 Labeling of fusion proteins of O<sup>6</sup>-alkylguanine-DNA alkyltransferase with small  
531 molecules in vivo and in vitro. *Methods* 32, 437–444.  
532 <https://doi.org/10.1016/j.ymeth.2003.10.007>

533 Kern, A., Albarran-Zeckler, R., Walsh, H.E., Smith, R.G., 2012. Apo-ghrelin receptor forms  
534 heteromers with DRD2 in hypothalamic neurons and is essential for anorexigenic  
535 effects of DRD2 agonism. *Neuron* 73, 317–332.  
536 <https://doi.org/10.1016/j.neuron.2011.10.038>

537 Kern, A., Mavrikaki, M., Ullrich, C., Albarran-Zeckler, R., Brantley, A.F., Smith, R.G., 2015.  
538 Hippocampal Dopamine/DRD1 Signaling Dependent on the Ghrelin Receptor. *Cell*  
539 163, 1176–1190. <https://doi.org/10.1016/j.cell.2015.10.062>

540 Kojima, M., Hosoda, H., Date, Y., Nakazato, M., Matsuo, H., Kangawa, K., 1999. Ghrelin is a  
541 growth-hormone-releasing acylated peptide from stomach. *Nature* 402, 656–660.  
542 <https://doi.org/10.1038/45230>

543 Leyris, J.-P., Roux, T., Trinquet, E., Verdié, P., Fehrentz, J.-A., Oueslati, N., Douzon, S.,  
544 Bourrier, E., Lamarque, L., Gagne, D., Galleyrand, J.-C., M'kadmi, C., Martinez, J.,  
545 Mary, S., Banères, J.-L., Marie, J., 2011. Homogeneous time-resolved fluorescence-  
546 based assay to screen for ligands targeting the growth hormone secretagogue  
547 receptor type 1a. *Anal. Biochem.* 408, 253–262.  
548 <https://doi.org/10.1016/j.ab.2010.09.030>

549 López Soto, E.J., Agosti, F., Cabral, A., Mustafa, E.R., Damonte, V.M., Gandini, M.A.,  
550 Rodríguez, S., Castrogiovanni, D., Felix, R., Perelló, M., Raingo, J., 2015.  
551 Constitutive and ghrelin-dependent GHSR1a activation impairs CaV2.1 and CaV2.2  
552 currents in hypothalamic neurons. *J. Gen. Physiol.* 146, 205–219.  
553 <https://doi.org/10.1085/jgp.201511383>

554 Lufrano, D., Trejo, S.A., Llovera, R.E., Salgueiro, M., Fernandez, G., Martínez Damonte, V.,  
555 González Flecha, F.L., Raingo, J., Ermácora, M.R., Perelló, M., 2016. Ghrelin binding  
556 to serum albumin and its biological impact. *Mol. Cell. Endocrinol.* 436, 130–140.  
557 <https://doi.org/10.1016/j.mce.2016.07.016>

558 Mani, B.K., Walker, A.K., Lopez Soto, E.J., Raingo, J., Lee, C.E., Perelló, M., Andrews, Z.B.,  
559 Zigman, J.M., 2014. Neuroanatomical characterization of a growth hormone  
560 secretagogue receptor-green fluorescent protein reporter mouse. *J. Comp. Neurol.*  
561 522, 3644–3666. <https://doi.org/10.1002/cne.23627>

562 Maurel, D., Comps-Agrar, L., Brock, C., Rives, M.-L., Bourrier, E., Ayoub, M.A., Bazin, H.,  
563 Tinel, N., Durroux, T., Prézeau, L., Trinquet, E., Pin, J.-P., 2008. Cell-surface protein-  
564 protein interaction analysis with time-resolved FRET and snap-tag technologies:  
565 application to GPCR oligomerization. *Nat. Methods* 5, 561–567.  
566 <https://doi.org/10.1038/nmeth.1213>

567 McEwen, D.P., Gee, K.R., Kang, H.C., Neubig, R.R., 2001. Fluorescent BODIPY-GTP  
568 analogs: real-time measurement of nucleotide binding to G proteins. *Anal. Biochem.*  
569 291, 109–117. <https://doi.org/10.1006/abio.2001.5011>

570 McGirr, R., McFarland, M.S., McTavish, J., Luyt, L.G., Dhanvantari, S., 2011. Design and  
571 characterization of a fluorescent ghrelin analog for imaging the growth hormone  
572 secretagogue receptor 1a. *Regul. Pept.* 172, 69–76.  
573 <https://doi.org/10.1016/j.regpep.2011.08.011>

574 M'Kadmi, C., Cabral, A., Barrile, F., Giribaldi, J., Cantel, S., Damian, M., Mary, S., Denoyelle,  
575 S., Dutertre, S., Péraldi-Roux, S., Neasta, J., Oiry, C., Banères, J.-L., Marie, J.,  
576 Perello, M., Fehrentz, J.-A., 2019. N-Terminal Liver-Expressed Antimicrobial Peptide  
577 2 (LEAP2) Region Exhibits Inverse Agonist Activity toward the Ghrelin Receptor. *J.*  
578 *Med. Chem.* 62, 965–973. <https://doi.org/10.1021/acs.jmedchem.8b01644>

579 Morin, V., Hozer, F., Costemale-Lacoste, J.-F., 2018. The effects of ghrelin on sleep,  
580 appetite, and memory, and its possible role in depression: A review of the literature.  
581 *Encephale* 44, 256–263. <https://doi.org/10.1016/j.encep.2017.10.012>

582 Paxinos, G., Franklin, K.B.J., 2001. *The mouse brain in stereotaxic coordinates*, 2nd ed.  
583 Academic Press, San Diego.

584 Perello, M., Cabral, A., Cornejo, M.P., De Francesco, P.N., Fernandez, G., Uriarte, M., 2018.  
585 Brain accessibility delineates the central effects of circulating ghrelin. *J.*  
586 *Neuroendocrinol.* e12677. <https://doi.org/10.1111/jne.12677>

587 Perello, M., Dickson, S.L., 2015. Ghrelin signalling on food reward: a salient link between the  
588 gut and the mesolimbic system. *J. Neuroendocrinol.* 27, 424–434.  
589 <https://doi.org/10.1111/jne.12236>

590 Perello, M., Scott, M.M., Sakata, I., Lee, C.E., Chuang, J.-C., Osborne-Lawrence, S.,  
591 Rovinsky, S.A., Elmquist, J.K., Zigman, J.M., 2012. Functional implications of limited  
592 leptin receptor and ghrelin receptor coexpression in the brain. *J. Comp. Neurol.* 520,  
593 281–294. <https://doi.org/10.1002/cne.22690>

594 Schaeffer, M., Langlet, F., Lafont, C., Molino, F., Hodson, D.J., Roux, T., Lamarque, L.,  
595 Verdié, P., Bourrier, E., Dehouck, B., Banères, J.-L., Martinez, J., Méry, P.-F., Marie,  
596 J., Trinquet, E., Fehrentz, J.-A., Prévot, V., Mollard, P., 2013. Rapid sensing of  
597 circulating ghrelin by hypothalamic appetite-modifying neurons. *Proc. Natl. Acad. Sci.*  
598 *U.S.A.* 110, 1512–1517. <https://doi.org/10.1073/pnas.1212137110>

599 Schellekens, H., De Francesco, P.N., Kandil, D., Theeuwes, W.F., McCarthy, T., van  
600 Oeffelen, W.E.P.A., Perelló, M., Giblin, L., Dinan, T.G., Cryan, J.F., 2015. Ghrelin's  
601 Orexigenic Effect Is Modulated via a Serotonin 2C Receptor Interaction. *ACS Chem*  
602 *Neurosci* 6, 1186–1197. <https://doi.org/10.1021/cn500318q>

603 Schindelin, J., Arganda-Carreras, I., Frise, E., Kaynig, V., Longair, M., Pietzsch, T.,  
604 Preibisch, S., Rueden, C., Saalfeld, S., Schmid, B., Tinevez, J.-Y., White, D.J.,  
605 Hartenstein, V., Eliceiri, K., Tomancak, P., Cardona, A., 2012. Fiji: an open-source  
606 platform for biological-image analysis. *Nat. Methods* 9, 676–682.  
607 <https://doi.org/10.1038/nmeth.2019>

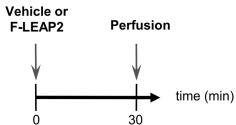
608 Scott, M.M., Perello, M., Chuang, J.-C., Sakata, I., Gautron, L., Lee, C.E., Lauzon, D.,  
609 Elmquist, J.K., Zigman, J.M., 2012. Hindbrain ghrelin receptor signaling is sufficient to  
610 maintain fasting glucose. *PLoS ONE* 7, e44089.  
611 <https://doi.org/10.1371/journal.pone.0044089>

612 Uriarte, M., De Francesco, P.N., Fernandez, G., Cabral, A., Castrogiovanni, D., Lalonde, T.,  
613 Luyt, L.G., Trejo, S., Perello, M., 2019. Evidence Supporting a Role for the Blood-  
614 Cerebrospinal Fluid Barrier Transporting Circulating Ghrelin into the Brain. *Mol.*  
615 *Neurobiol.* 56, 4120–4134. <https://doi.org/10.1007/s12035-018-1362-8>

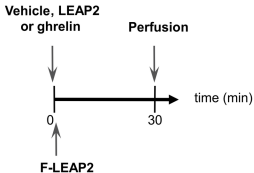
616 Wang, J.-H., Li, H.-Z., Shao, X.-X., Nie, W.-H., Liu, Y.-L., Xu, Z.-G., Guo, Z.-Y., 2019.  
617 Identifying the binding mechanism of LEAP2 to receptor GHSR1a. *FEBS J.* 286,  
618 1332–1345. <https://doi.org/10.1111/febs.14763>

619 Zigman, J.M., Jones, J.E., Lee, C.E., Saper, C.B., Elmquist, J.K., 2006. Expression of ghrelin  
620 receptor mRNA in the rat and the mouse brain. *J. Comp. Neurol.* 494, 528–548.  
621 <https://doi.org/10.1002/cne.20823>  
622

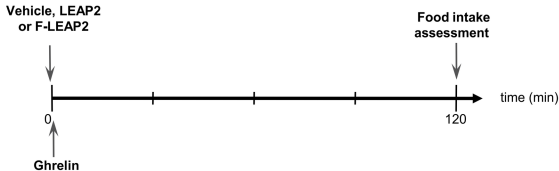
**A.** *In vivo* experiment 1

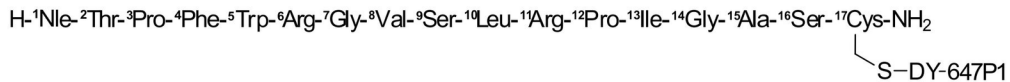
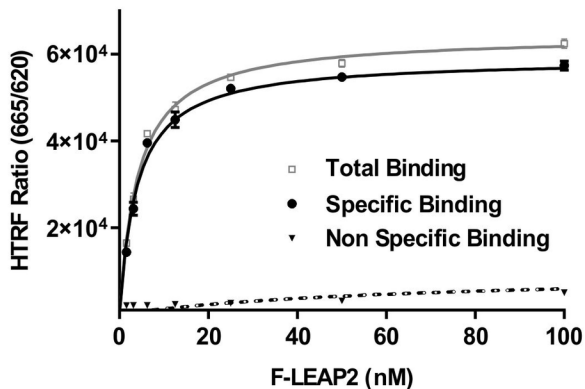
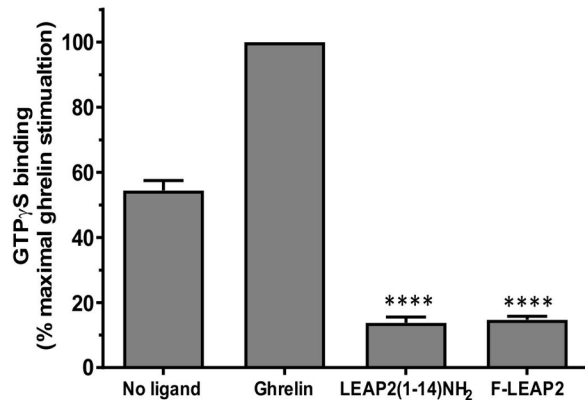


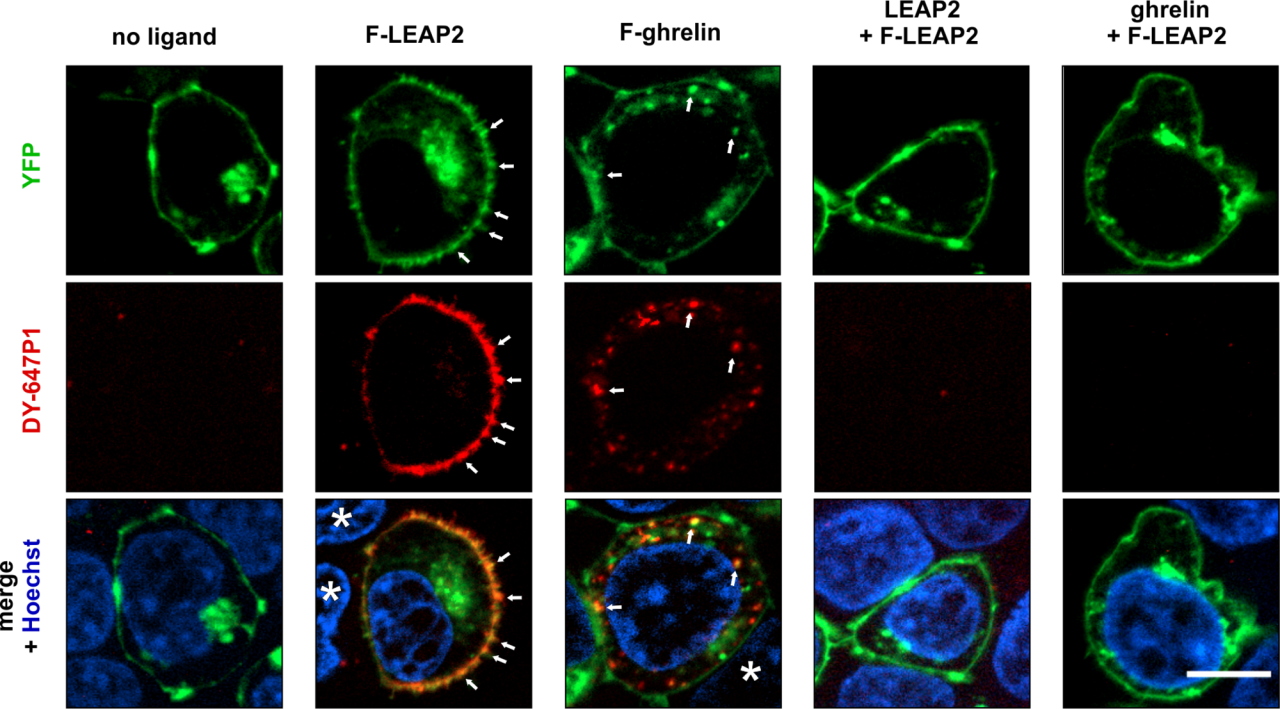
**B.** *In vivo* experiment 2

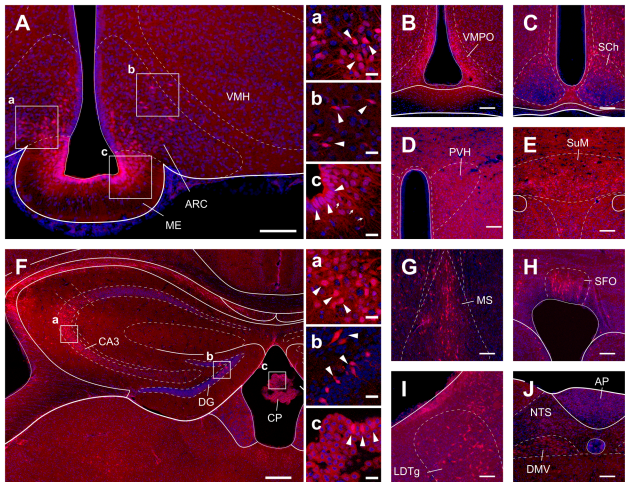


**C.** *In vivo* experiment 3

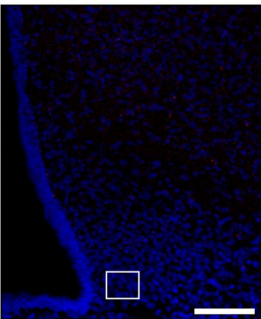


**A****B****C**

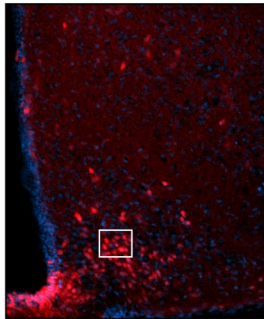




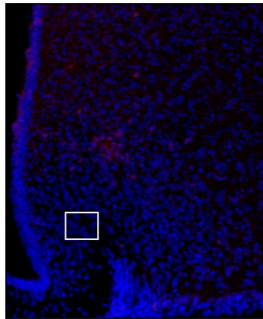
**Vehicle**



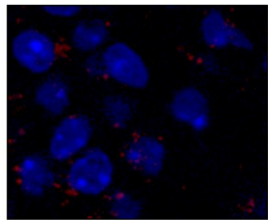
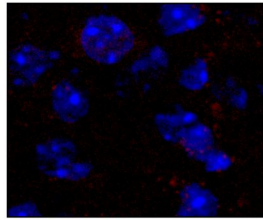
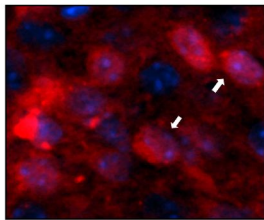
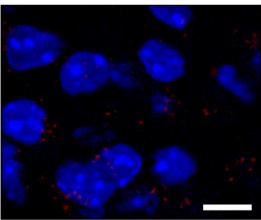
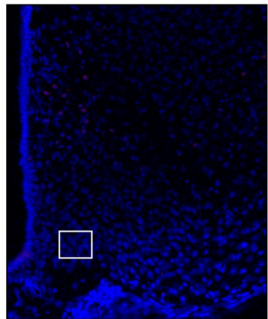
**F-LEAP2**



**LEAP2  
+ F-LEAP2**



**Ghrelin  
+ F-LEAP2**



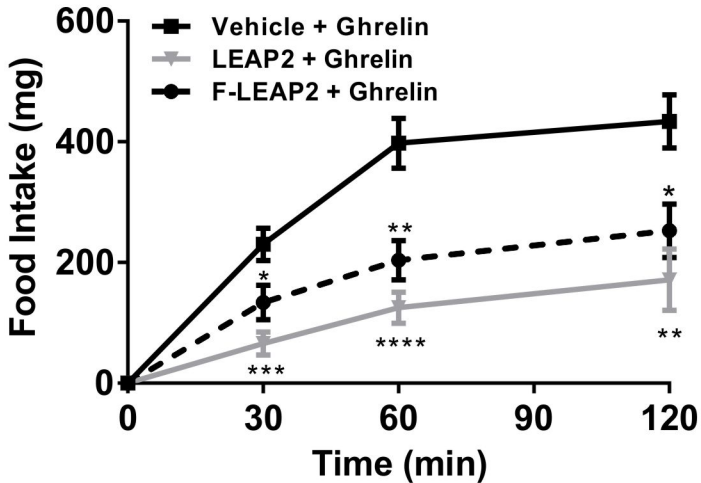


**TABLE 1.** Brain areas with fluorescent signal in mice ICV-injected with F-LEAP2<sup>1</sup>. The abbreviations listed in Table 1 are used in the text and in Figure 3.

<b>Hippocampus and septum</b>	
Ammon's horn, CA1	+/-
Ammon's horn, CA2	+
Ammon's horn, CA3	+++
Dentate gyrus –DG	++
Media septal –MS	+
<b>Thalamus</b>	
Paraventricular thalamic nucleus –PV	+
<b>Hypothalamus</b>	
Anterior hypothalamic area –AHA	+
Arcuate hypothalamic nucleus –ARC	+++
Dorsomedial nucleus –DMH	+
Paraventricular nucleus –PVH	++
Periventricular hypothalamic nucleus –Pe	+
Premamillary nucleus, ventral –PMV	+
Supramammillary nucleus –SuM	++
Suprachiasmatic nucleus –Sch	++
Ventromedial nucleus –VMH	++
Ventromedial preoptic nucleus –VMPO	++
Subfornical organ –SFO	++
<b>Midbrain, pons, and medulla oblongata</b>	
Area postrema –AP	++
Dorsal motor nucleus of the vagus –DMNV	++
Dorsal raphe nucleus –DR	+/-
Dorsal tegmental nucleus –DTg	+/-
Edinger Westphal nucleus –EW	+/-
Laterodorsal tegmental nucleus –LDTg	+
Magnocellular nucleus of the posterior commissure –MCPC	+/-
Nucleus ambiguous –Amb	-
Nucleus of the solitary tract –NTS	+
Parabrachial nucleus –PBN	+/-
Substantia nigra –SN	+/-
Ventral tegmental area –VTA	+/-

<sup>1</sup> Qualitative estimates of F-LEAP2 signal were made by considering both signal strength and the number of labeled cells: +++, high density; ++, moderate density; +, low density; +/-, inconsistent visualization.